Far-Field Interrogation of Microstrip Patch Antenna for Temperature Sensing Without Electronics

Jun Yao, *Student Member, IEEE*, Franck Mbanya Tchafa, *Student Member, IEEE*, Ankur Jain, Saibun Tjuatja, *Senior Member, IEEE*, and Haiying Huang, *Member, IEEE*

***Abstract*— Temperature sensing without electronics is demonstrated through wireless interrogation of passive antenna-sensors. The sensor node is equipped with an ultra-wide-band microstrip antenna as the transmitting/receiving (Tx/Rx) antenna and a microstrip patch antenna serving as the temperature-sensing element. A microstrip transmission line connecting the Tx/Rx antenna and the antenna-sensor delays the signal reflected from the sensing element and thus separated it from the background clutter. The operation principle of the wireless sensing scheme is first discussed, followed by the design and simulations of the sensor node circuitry. A digital signal processing algorithm that extracts the antenna resonant frequency from the wirelessly received signal is also described. Temperature tests were conducted to validate the performance of the wireless antenna sensor inside an oven.**

***Index Terms*— Wireless interrogation, passive wireless sensor, temperature sensor, UWB antenna, antenna-sensor, condition monitoring.**

I. Introduction

TEMPERATURE sensing is important inside many industrial production environments to optimize their operation parameters and to ensure safety. Due to their harsh environments, conditioning monitoring of these machines is extreme challenging. Wired temperature sensors, such as thermocouples [1] and optical fiber sensors [2] are commonly used. However, cables and connectors that can sustain high temperatures are expensive and prone to failure [3]. Various wireless temperature sensing techniques have been developed in recent years to eliminate the wiring requirements. Base on their configurations, wireless temperature sensors can be classified into two categories: the ones with electronic chips on board (i.e. the chip-based wireless sensors) or the ones without any electronic chips (i.e. the chipless wireless sensors). Most chip-based wireless sensors are designed based on the Berkeley mote platform [4], in which a microcontroller controls the data acquisition, signal processing, as well as the wireless data transmission [5], [6]. As such, these wireless sensors also need an on-board battery to power the microcontroller and the associated peripherals. Another group of chip-based wireless sensors is based on the Radio Frequency Identification (RFID) technology. A Wireless Identification and Sensing Platform (WISP) were presented in [7]. Similar to the mote-based wireless sensors, the WISP acquires the analog outputs of external sensors and converts them into digital data. The digital sensing data are then wirelessly transmitted by modulating the backscattered interrogation signal. As such, the WISP does not have a wireless transmitter on board and thus can operate on energy harvested from the interrogation signal. The power consumption of the RFID-based temperature sensors can be further reduced by implementing a complementary metal-oxide semiconductor (CMOS) temperature sensor that directly modulates the backscattered signal without any digitization [8]. One common limitation of the chip-based wireless sensors is that they can only operate at temperatures below the temperature limit of the electronic chips. At higher temperatures, chipless wireless sensors are the only feasible solution. Reindl and Shrena [9] demonstrated a remote temperature sensing system using a Surface Acoustic Wave (SAW) sensor and a passive dipole antenna, in which a radio frequency (RF) signal is received by the antenna and passed on to an interdigital transducer (IDT) to generate SAWs in the piezoelectric substrate. A reflector placed at a distance from the IDT reflects the SAWs back to the IDT, which is subsequently converted to RF signals and retransmitted by the dipole antenna. Temperature is then measured from the SAW speed that is extracted from the wirelessly received signal. The low operation frequency of the SAW sensors, however, makes sensor miniaturization extremely difficult. Chipless RFID sensors are another alternative for passive wireless temperature sensing. In [10], a resistive temperature sensor was implemented as the load of a UWB antenna. Due to the impedance mismatch between the resistive load and the antenna, the amplitude of the antenna backscattering is modulated as a function of temperature. Unfortunately, the antenna backscattering is also influenced by the distance and orientation between the reader and the sensor. Therefore, it is difficult to achieve calibrated sensor measurements using such a configuration. Self-calibrated wireless temperature sensor was achieved by connecting an RF cavity resonator to an antenna and temperature can be measured from the shift of the resonant frequency using a time-domain (TD) gating technique [11]. A dielectric resonator made of zirconium tintitanate was also studied for wireless temperature sensing [12]. Since the resonator can retain a Quality (Q) factor higher than 670 at 700 °C, far-field sensing of its resonator frequency up to 1.2 m was achieved. The major limitation of a dielectric resonator is that its Q factor decreases

Manuscript received June 21, 2016; accepted July 26, 2016. Date of publication August 2, 2016; date of current version September 1, 2016. This work was supported by the Department of Energy under Award DE-FE0023118. The associate editor coordinating the review of this paper and approving it for publication was Prof. Boby George.

J. Yao and S. Tjuatja are with the Department of Electric Engineering, University of Texas at Arlington, Arlington, TX 76019 USA (e-mail: jun.yao@mavs.uta.edu; tjuatja@uta.edu).

F. Mbanya Tchafa, A. Jain, and H. Huang are with the Department of Mechanical and Aerospace Engineering, University of Texas at Arlington, Arlington, TX 76019 USA (e-mail: franckeric.mbanyatchafa@mavs.uta.edu; jaina@uta.edu; huang@uta.edu).

Digital Object Identifier 10.1109/JSEN.2016.2597739

1558-1748 © 2016 IEEE. Personal use is permitted, but republication/redistribution requires IEEE permission.
See http://www.ieee.org/publications_standards/publications/rights/index.html for more information.

as the temperature increases [12], [13]. Thus, the radiated power from the resonator decays quickly at higher temperatures, which makes far-field sensing difficult. Besides, a dielectric resonator is usually quite bulky. Another chipless wireless temperature sensor is the coupled Inductive-Capacitive (LC) resonance sensor [14], [15]. Temperature affects the resonant frequency of the LC sensor and its frequency can be wirelessly detected via inductive coupling between the sensor and the reader coils. The interrogation distance of LC resonant sensors, however, is only a few centimeters since the coils of the sensor and reader have to be placed in the near fields of each other.

Significant researches have been conducted on the antenna-sensor technology due to its planar configuration, low-cost, passive operation, and multi-modality sensing capabilities [16]. Since the antenna-sensor has a simple and conformal planar configuration, it can be easily attached on the structure surfaces for Structure Health Monitoring (SHM) [17]. Several wireless interrogation techniques have been developed for the antenna sensors, including normalized Time Domain Reflectometry (TDR) [18] and RFID-enabled techniques [19]–[21]. High-speed wireless interrogation of the antenna-sensor was achieved using an amplitude modulator and a Frequency Modulated Continue Wave (FMCW) interrogator [22]. Similar to the RFID sensors, the wireless interrogation mechanisms developed so far require electronics in the sensor node, which limits their applications in high-temperature environments. In order to use an antenna-sensor for high temperature sensing, wireless sensor nodes without electronics have to be developed. A near-field interrogation mechanism for a chipless antenna-sensor was proposed in [23]. The patch antenna-sensor was directly interrogated without using any electronics. However, since the patch-antenna has a relative low Q factor [24], the maximum wireless interrogation distance achieved was only 5 cm.

In this study, far-field interrogation of an antenna-sensor without electronics was demonstrated for temperature sensing. The sensor node consists of a microstrip patch antenna serving as the temperature sensing unit [25] and a UWB transmitting/receiving (Tx/Rx) antenna with a Reactive Impedance Surface (RIS) ground plane [26], [27]. While other passive wireless sensors usually have an antenna as a data communication device, to the best of our knowledge, the presented work is the first in employing the microstrip antenna as a wireless temperature sensing element. By doing so, the entire sensor node can be implemented on a commercial printed circuit board (PCB) using simple fabrication techniques such as chemical etching. The temperature information is encoded in the signals backscattered by the antenna sensor and a TD gating technique is developed to extract the resonant frequency of the antenna sensor from the backscattered signal.

II. Principle of Operation

A. Patch Antenna for Temperature Sensing

Assume a rectangular patch antenna operates in the TM_{010} mode, its resonant frequency f_{res} can be calculated based on the transmission line model [28], i.e.

$$f_{res} = \frac{c}{2L_e\sqrt{\varepsilon_r}}, \tag{1}$$

where c is the speed of light and ε_r is the dielectric constant of the substrate material. L_e is the electrical length of the patch antenna, which equals to the physical length L of the radiation patch approximately, i.e. $L_e \approx L$. The resonant frequency variation δf_{res} can then be expressed in terms of the changes in the substrate dielectric constant ε_r and the patch length L as

$$\delta f_{res} = \frac{\partial f_{res}}{\partial \varepsilon_r}\delta\varepsilon_r + \frac{\partial f_{res}}{\partial L}\delta L. \tag{2}$$

We can also derive from equation (1) that

$$\frac{\partial f_{res}}{\partial \varepsilon_r} = \left(-\frac{1}{2\varepsilon_r}\right) f_{res} \tag{3}$$

and

$$\frac{\partial f_{res}}{\partial L} = \left(-\frac{1}{L}\right) f_{res}. \tag{4}$$

Substituting equations (3) and (4) into (2) and normalizing the resonant frequency shift with the antenna's resonant frequency, we obtain

$$\frac{\delta f_{res}}{f_{res}} = -\frac{1}{2}\frac{\delta\varepsilon_r}{\varepsilon_r} - \frac{\delta L}{L}. \tag{5}$$

For the purpose of temperature sensing, equation (5) can be expressed in terms of temperature change δT as

$$\frac{\delta f_{res}}{f_{res}} = -\frac{1}{2}\alpha_\varepsilon\delta T - \alpha_T\delta T = \left(-\frac{1}{2}\alpha_\varepsilon - \alpha_T\right)\delta T = K_T\delta T, \tag{6}$$

where α_ε is the thermal coefficient of the substrate dielectric constant; α_T is its coefficient of thermal expansion. K_T is defined as the temperature sensitivity of the normalized frequency shift and is a linear function of α_ε and α_T.

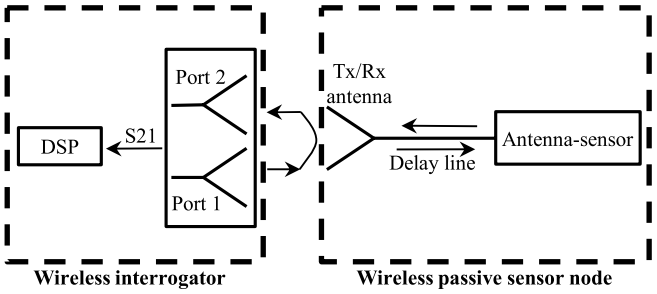

Fig. 1. Block diagram of the wireless temperature sensing system.

B. Wireless Interrogation Based on Antenna Backscattering

The wireless sensing system can be separated into two subsystems: a wireless interrogator and a passive wireless sensor node, as shown in Fig. 1. The sensor node consists of a patch antenna-sensor and a UWB Tx/Rx antenna connected with a microstrip transmission line. The Tx/Rx antenna is used

to receive the wide band interrogation signal from the interrogator and re-broadcast the signals reflected by the antenna sensor (i.e. the antenna sensor backscattering) back to the wireless interrogator. To avoid the self-jamming problem [16], the microstrip transmission line is used to introduce a time delay between the background clutter, including the Tx/Rx antenna backscattering, and the antenna sensor backscattering. As long as the transmission line is of sufficient length, the antenna reflection can be distinguished from the background clutter in the time domain.

The wireless interrogator is based on measuring the two-port transmission scattering parameter, i.e. the S21 parameter, between the two interrogation antennas. A linear chirp interrogation signal was generated and broadcasted to the passive wireless sensor through the interrogation antenna connected to port 1 of the interrogator. This interrogation signal is received by the UWB Tx/Rx antenna of the sensor node and transmitted to the antenna-sensor via the microstrip delay line. Upon reaching the antenna-sensor, the portion of the interrogation signal that matches the antenna resonant frequency is received and radiated by the antenna-sensor. The remaining interrogation signal is reflected by the antenna sensor and broadcasted back to the interrogator via the Tx/Rx antenna. As such, the reflection coefficient of the antenna-sensor is encoded into the backscattered signal. The power of the antenna backscattering received by the interrogator can be calculated using Friis equation as

$$P_r = P_t G_{it} G_{ir} G_s^2 \left(\frac{\lambda}{4\pi d}\right)^4 S_{11} L_d, \tag{7}$$

where P_t is the power of the transmitted interrogation signal; d is the distance between the wireless interrogator and the Tx/Rx antenna; G_{it} and G_{ir} are the radiation gains of the interrogator Tx/Rx antennas; G_s is the radiation gain of the UWB sensor antenna; λ is the wavelength of the interrogation signal; S_{11} is the reflection coefficient of the antenna-sensor and L_d is the loss introduced by the delay line. The minimum detectable power of the wireless interrogator can be expressed as [11]:

$$P_{r\,\min} = E \cdot B \cdot F \cdot SNR, \tag{8}$$

where E is the thermal energy; $B$is the bandwidth of the receiver; $F$is the noise figure of the interrogator receiver and SNR is the required signal to noise ratio for this system. Substituting (7) into (8), the theoretical maximum interrogation distance can be calculated as

$$d_{\max} = \frac{\lambda}{4\pi}\left(\frac{P_t G_{tt} G_{tr} G_r^2 S_{11} L_d}{E \cdot B \cdot F \cdot SNR}\right)^{\frac{1}{4}}. \tag{9}$$

Based on equation (9), the maximum interrogation distance is estimated to be 2.25 m assuming a transmitted power of 10 dBm, $E = 4 \times 10^{-21}$ J, $B = 0.8$ GHz, $SNR = 20$ dB, $G_{it} = 12$ dBi, $G_{ir} = 12$ dBi, $G_r = 4$ dBi, $L_d = -1$ dB, $S_{11} = -10$ dB, $F = 1$ dB, and a wavelength of 0.12 m.

Once the interrogator receives the backscattered signals, including the antenna sensor backscattering and the background clutter, it is processed by a digital signal processing (DSP) program to separate the antenna sensor backscattering from the background clutter. Frequency analysis can then be performed on the antenna sensor backscattering to extract the resonant frequency of the antenna sensor.

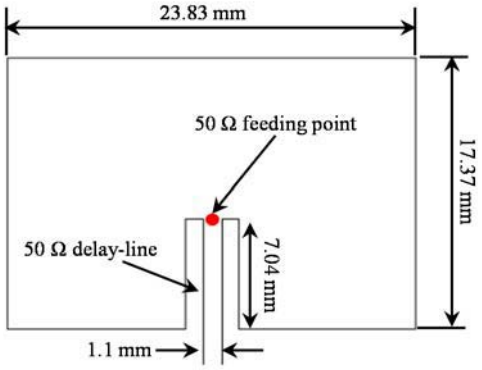

Fig. 2. Physical dimensions and feeding structure of the designed microstrip antenna-sensor.

III. Sensor Node Implementation

A. Design of Temperature Antenna-Sensor

A commercial high frequency circuit laminate, Rogers RO3210 [29], was selected as the substrate material for the wireless sensor because of its high thermal coefficient of dielectric constant α_ε, which is -459 ppm/°C in the temperature range from 0°C to 100°C. Compare to α_ε, its thermal expansion coefficient α_T of 13 ppm/°C is much smaller. Based on equation (6), the theoretical temperature sensitivity of the normalized frequency shift K_T is calculated to be 216.5 ppm/°C. Since RO3210 is a ceramic-filled laminates reinforced with woven fiberglass, its operation temperature is limited by the transition temperature (Tg) of the fiberglass, which is 350°C.

The radiation patch of an antenna-sensor with a designed frequency of 2.45 GHz is shown in Fig. 2. The radiation patch is fed with a 50 Ω microstrip transmission line to excite the fundamental radiation mode along the width direction. In order to obtain a good impedance matching between the transmission line and the radiation patch, the inset fed structure was used. The 50 Ω feeding point was calculated to be at 7.04 mm above the bottom edge of the radiation patch. The length of the transmission line was selected to be 200 mm to ensure sufficient separation between the UWB Tx/Rx antenna and the antenna sensor.

To confirm the antenna design, a three-dimensional (3D) model of the designed antenna-sensor was developed in High Frequency Structure Simulator (HFSS). For a substrate dielectric constant of 10.8 at room temperature (20°C), every 20°C increase in temperature will reduce the dielectric constant by 10.8*459 ppm/°C * 20°C = 0.1. Thus, the substrate dielectric constant of the simulation model was varied from 10.9 to 10.4 with a step of -0.1, which corresponds to temperature changes from 0°C to 100°C. The simulated resonant frequencies were normalized with respect to the frequency at room temperature and are plotted versus the temperature in Fig. 3. The simulated curve displays a high degree of linearity

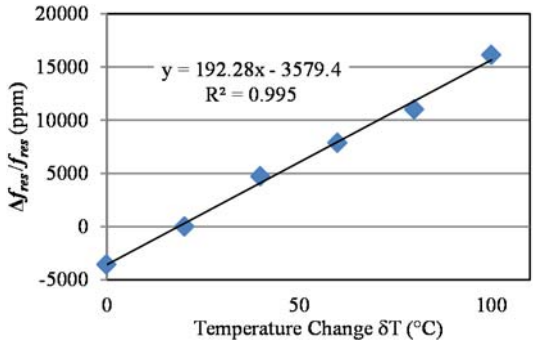

Fig. 3. Simulated relationship between the antenna-sensor's normalized resonant frequency shift and the temperature.

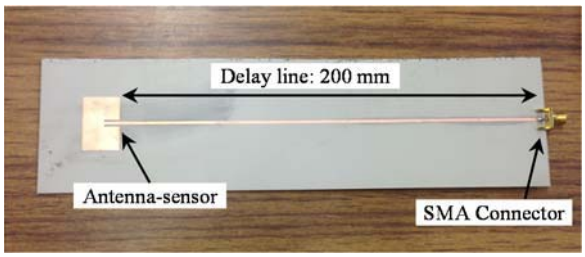

Fig. 4. Fabricated antenna-senor with the microstrip delay line.

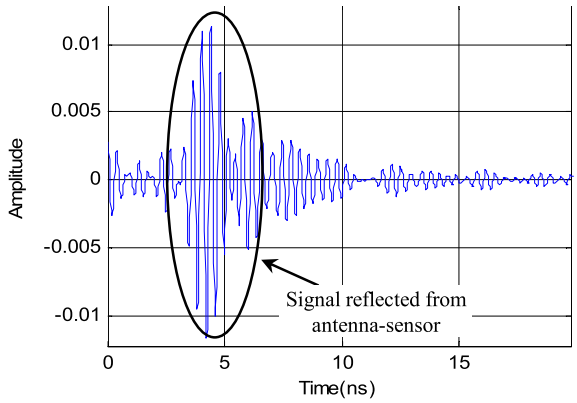

Fig. 5. Time domain signal converted from the measured S11 parameter of the fabricated antenna-sensor with the delay line.

(coefficient of determination $R^2 = 0.995$) and the resulting temperature sensitivity K_T, i.e. the slope of the trend line, is 192.3 ppm/°C, which is slightly lower than the value of 216.5 ppm/°C predicted by the transmission line model.

The antenna-sensor and the delay line were fabricated using a chemical etching technique, as shown in Fig. 4. In order to characterize the round-trip time delay caused by the delay line, a 50 Ω Subminiature version A (SMA) connector was soldered on the end of delay line. The S11 parameter of the fabricated antenna-sensor was firstly measured using a Vector Network Analyzer (VNA) and then converted to the time domain response represented in Fig. 5. The wave packet corresponding to the antenna backscattering starts at 3.5 ns, which is the round-trip time delay between the SMA connector and the antenna-sensor.

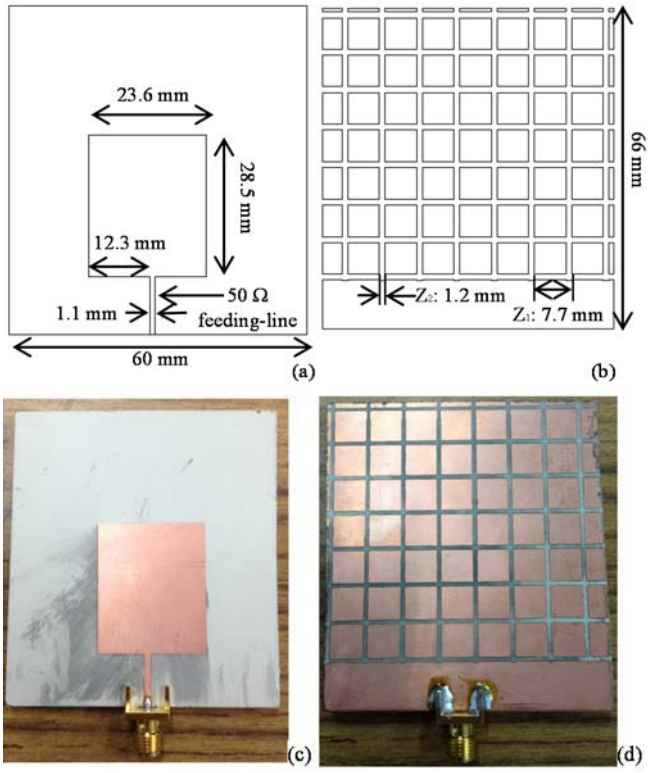

Fig. 6. UWB Tx/Rx antenna: (a) dimensions of the radiation patch; (b) dimensions of the ground plane; (c) top view of the fabricated antenna; and (d) bottom view of the fabricated antenna.

B. Design of UWB Tx/Rx Microstrip Antenna

To implement the entire sensor node on printed circuit boards, the UWB Tx/Rx antenna was developed based on a one-layer substrate patch antenna. The radiation patch is a conventional rectangular patch fed at the bottom edge using a 50 Ω microstrip transmission line, as shown in Fig. 6(a). The ground plane, on the other hand, has a grid pattern with periodically crossed gaps that divide the metallic ground into small square patches (see Fig. 6(b)). The patterned ground plane and the rectangular radiation patch can be considered as a type of metamaterial, namely a RIS structure that acts like a parallel LC resonant circuit [27]. The resonant frequency f_{RIS} of the LC circuit can be determined when it has the largest impedance. The impedance of the LC circuit can be expressed by the impedance of the equivalent inductor X_L and capacitor X_C, i.e.

$$Z_{LC} = j\frac{X_L X_C}{X_C - X_L}, \tag{10}$$

where X_L and X_C can be calculated as

$$X_L = Z_d \tan(kd) \tag{11}$$

and

$$X_c = \frac{K\,(Z_1/Z_2)}{2\pi f \varepsilon \times \sqrt{1-(Z_1/Z_2)^2} \times (Z_2 - Z_1)}. \tag{12}$$

In which, Z_d and k are the wave impedance and the propagation constant of the substrate material, respectively; d is the substrate thickness; Z_1 andZ_2, as shown in Fig. 6(b),

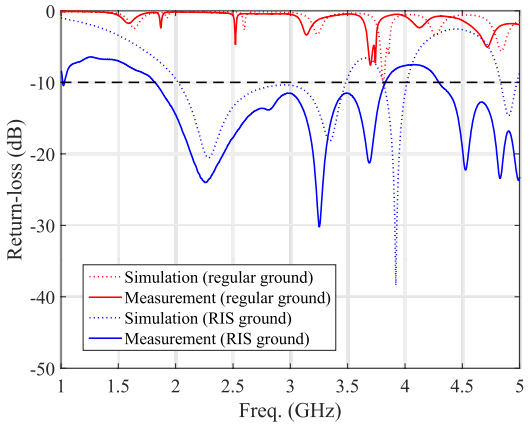

Fig. 7. Comparison between the simulated and measured S11 parameter of the UWB Tx/Rx antenna.

define the vertical coordinates of the strip edges; the function $K()$ is a complete elliptic integral which is defined in [26]. The RIS structure is inductive at frequencies below f_{RIS} while the radiation patch becomes capacitive below its resonant frequency f_{patch}. Therefore, by setting f_{RIS} higher than f_{patch}, the magnetic energy stored in the RIS structure can compensate for the electrical energy stored in the near field of the patch antenna, which results in additional resonances at lower frequencies and thus broaden the bandwidth of the antenna [27].

The design of the UWB Tx/Rx antenna started with a conventional patch antenna having a perfect ground plane. The resonant frequency of the conventional patch antenna f_{patch} was chosen to be at 3.8 GHz and the resonant frequency of the RIS structure f_{RIS} was selected as 4.2 GHz, which is slightly higher than f_{patch}. Base on the properties of the substrate material and the selected f_{RIS}, the dimensions of the patterned ground, i.e. Z_1 and Z_2, can be calculated to be 1.2 mm and 7.7 mm, respectively, using equation (10), (11) and (12).

The pictures of the radiation patch and the patterned ground plane of the UWB Tx/Rx antenna, fabricated using the chemical etching technique, are shown in Fig. 6(c) and 6(d). The S11 parameter of the fabricated antenna was measured and compared with the simulation results in Fig. 7. The bandwidth of the UWB Tx/Rx antenna, determined at the -10 reflection coefficient, is 1.6 GHz (i.e. from 1.9 to 3.5 GHz), which matches with the simulation very well. Compare to the conventional patch antenna, the -10 dB operation bandwidth of the metamaterial antenna increases by more than 100 times. The gain of the Tx/Rx antenna, measured using a two-port transmission test, is shown in Fig. 8. The antenna displayed a relatively flat gain, varying from 3.3 to 4 dBi in frequencies ranging from 2.2 GHz to 3 GHz. Due to its flat gain and wide bandwidth, the temperature sensitivity of the Tx/Rx antenna will have very little effect on the measurement of the antenna sensor resonant frequency.

After validating the performances of the antenna sensor and the Tx/Rx antenna separately using SMA connectors, both antennas were integrated on one RO3210 laminate by connecting them using a 200 mm microstrip transmission line. The entire sensor node was fabricated using chemical etching

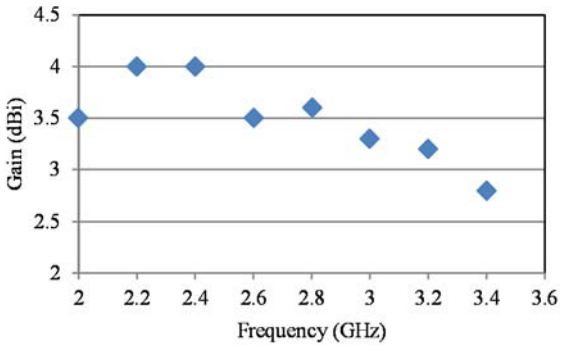

Fig. 8. Measured radiation gain of the fabricated UWB Tx/Rx antenna.

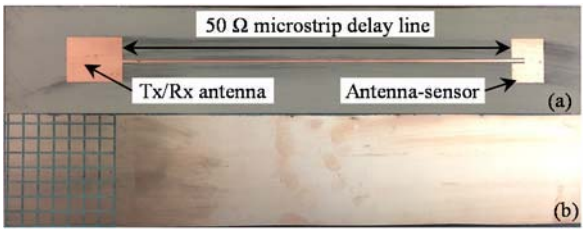

Fig. 9. Fabricated wireless temperature sensor node: (a) top view and (b) bottom view.

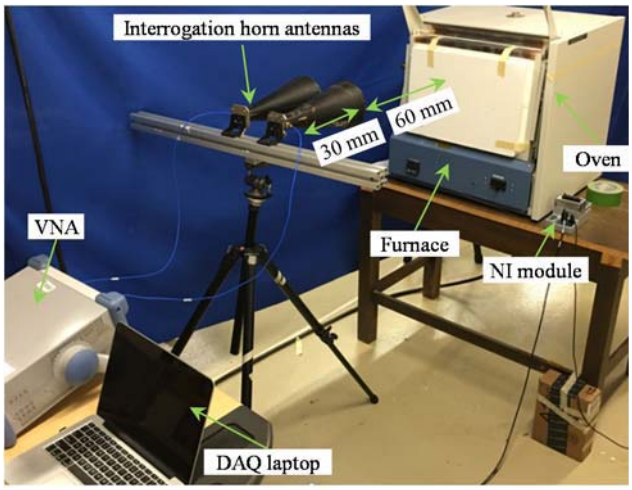

Fig. 10. Experimental setup for thermal testing.

and the pictures of its front and back surfaces are shown in Fig. 9.

IV. Instrumentation and Experimental Setup

A. Hardware Setup

The experimental setup for validating the temperature sensing capability of the antenna sensor as well as its wireless interrogation is shown in Fig. 10. The sensor node was placed inside an oven so that the environment temperature can be precisely controlled. For wireless interrogation, the metal panel of the oven door was removed but the insulation element was kept in place to prevent heat convection so that a stable temperature can be maintained inside the oven. The insulation element of the oven is made of a high temperature material that has a dielectric constant similar to air. Therefore, the insulation material will not introduce any additional changes on the phase or amplitude of the interrogation signal. The wireless

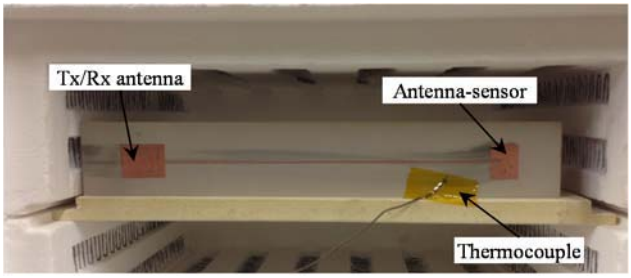

Fig. 11. Wireless sensor node placed at the entrance of the oven.

interrogator was realized by using a VNA and two horn antennas. The horn antennas were placed at an interrogation distance of 60 cm in front of the temperature oven facing the Tx/Rx antenna. These two horn antennas were connected to a two-port VNA using co-axial cables so that the transmitting S-parameter, i.e. the S21 parameter, can be acquired. The VNA was calibrated up to the feeding points of the interrogation antennas, which was 30 cm from the aperture of the interrogation antenna. Therefore, the wireless transmission distance between the feeding points of the integration antennas and the sensor node was 90 cm.

The sensor node was placed near the entrance of the temperature oven, as shown in Fig. 11. A T-type thermocouple was installed adjacent to the antenna-sensor to obtain the reference temperature. The thermocouple measurements were acquired using a National Instruments (NI) thermocouple module. Both the NI thermocouple module and the VNA were connected to a laptop; the communication between the laptop and the VNA was achieved via a wired local-area-network (LAN) connection while the communication between the computer and the NI module was achieved via a Universal Serial Bus (USB) connection. A LabVIEW program was developed to control the VNA and the NI module. The VNA was programmed to acquire the S21 parameters with a frequency resolution of 200 kHz over a frequency range of 2.2 to 3 GHz. The interrogation power was set to be 10 dBm. The S21 parameters were recorded every 2.3 seconds. At the meantime, the thermocouple readings were recorded every 0.1 second. Both recorded data were time stamped for easily correlation between the thermocouple readings and the resonant frequency extracted from the S21 parameters.

V. Digital Signal Processing

A DSP algorithm was developed to extract the resonant frequency of the antenna-sensor from the measured S21 parameters. The flow chart of the DSP algorithm is shown in Fig. 12(a) and the signals corresponding to each block are shown sequentially in Fig. 12(b). First, the acquired S21 parameter, which has a frequency range from f_1 to f_2, is zero padded from the direct current (DC) frequency (i.e. 0 Hz) to f_1. The zero-padded S parameter is then converted to a time-domain signal using Inverse Fast Fourier Transform (IFFT) [30]. As shown in Fig. 12(b), the resulting time-domain signal displays two major wave packets that correspond to the structural backscattering and the antenna sensor backscattering. Both wave packets have small side lobes, which can be reduced by windowing before the IFFT.

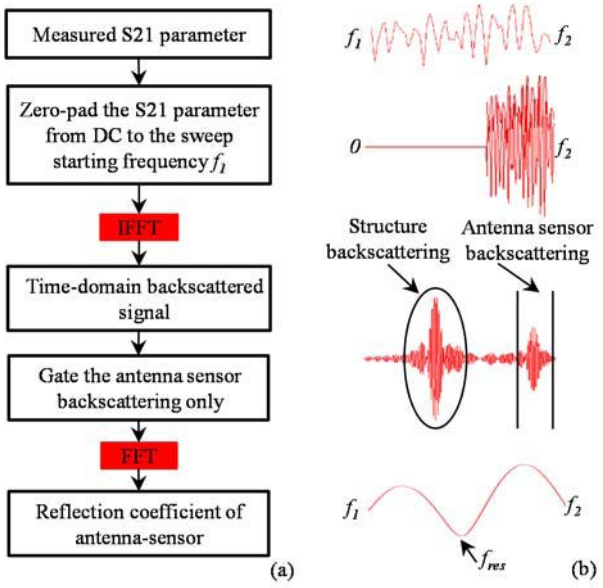

Fig. 12. Digital signal processing algorithm: (a) flow diagram and (b) signals corresponding to processing blocks.

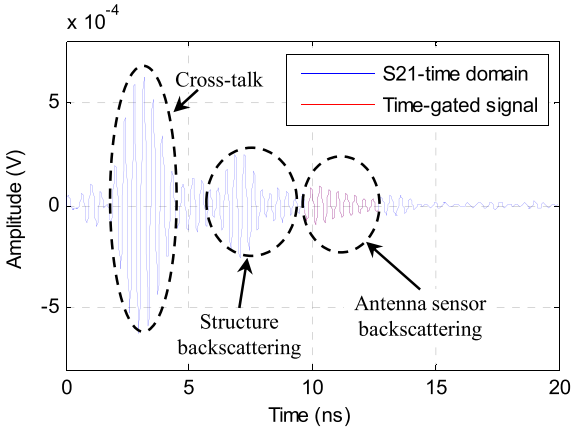

Fig. 13. Time-domain backscattered signal converted from the measured S21 parameter.

Nonetheless, the presents of the side lobes will not have an effect on determining the frequency of the antenna sensor backscattering. Even though the signals backscattered by the Tx/Rx antenna and the surrounding structures usually have the largest amplitude, they appear at a different time span from that of the antenna sensor backscattering. Therefore, a gating window can be applied to the time domain signal to extract the antenna sensor signal. Since the time-gated signal will only contain signals that are reflected at or near the feeding point of the antenna sensor, the time gating process also eliminate reflections at other locations along the transmission delay line due to temperature gradient, etc. Subsequently, the gated signal is converted back to the frequency domain using Fast Fourier Transform (FFT) and the resonant frequency of the antenna-sensor can be determined as the frequency at which the reflection coefficient has the lowest value.

VI. Results and Discussions

The time-domain representation of a typical S21 parameter is shown in Fig. 13. Time "0" corresponds to the feeding point

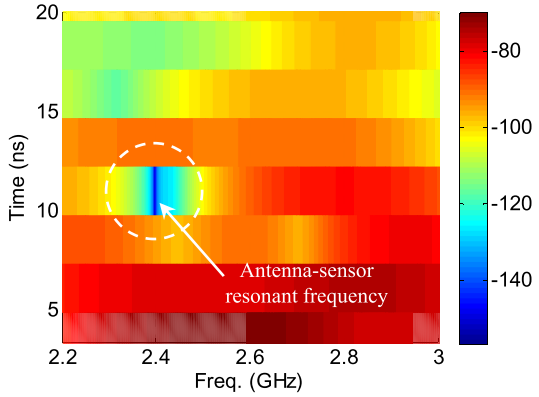

Fig. 14. Spectrogram of the backscattered signal.

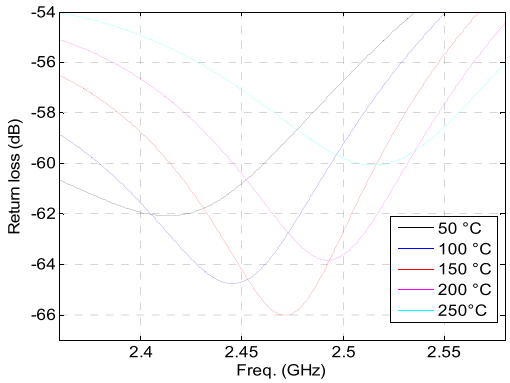

Fig. 15. Spectra of the gated time-domain signals at different temperatures.

of the transmitting interrogation horn antenna. The first wave packet arrives at around 2 ns, which corresponding to a round trip distance of 0.3 m in air. This distance coincides with the distance between the feeding point of the interrogation antenna and the antenna aperture. Therefore, we can conclude that this wave packet is due to the cross-talk between the two interrogation horn antennas. The second wave package arrives at around 6 ns, which corresponds to a round-trip distance of 0.9 m in air and thus is the structure mode backscattering generated by the Tx/Rx antenna and the temperature oven. The antenna sensor backscattering occurs at around 9.5 ns. The time difference between the structure mode and the antenna sensor mode is therefore around 3.5 ns, which matches with the delay time introduced by the transmission line very well. In addition, we can also determine the antenna sensor backscattering from the spectrogram of the backscattered signal. The signal backscattered by the antenna sensor should have a low amplitude at its resonant frequency while the structure mode backscattering usually have frequency components over the entire interrogation bandwidth. As shown in Fig. 14, the spectrogram of the backscattered signal, calculated using Short Time Fourier Transform (STFT), has a low energy band at around 2.4 GHz starting from 9.5 ns to 12.5 ns, which is the designed antenna resonant frequency. At other time windows, the energy are spread over large frequency spans. Therefore, we can easily determine that the starting and stopping time of the time gating window should be at 9.5 ns and 12.5 ns. The frequency spectra of the time gated signal at different temperatures are shown in Fig. 15. The resonant frequency

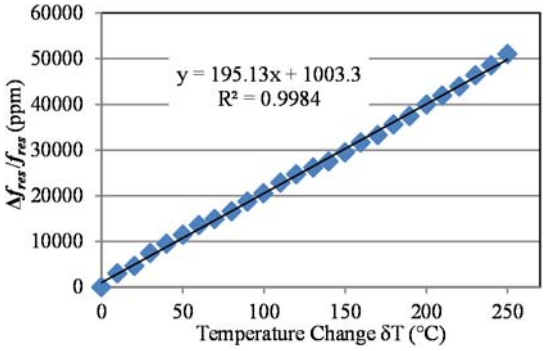

Fig. 16. Measured relationship between the antenna-sensor's normalized resonant frequency shift and the temperature change.

of the antenna sensor is determined as the frequencies at which the frequency spectrum has the lowest amplitude. The frequency shifts at different temperatures were normalized with respect to the resonant frequency of the antenna-sensor at room temperature. The measured normalized frequency shifts are plotted versus the temperature change measured from the thermocouple in Figure 16. The measurement data display a high degree of linearity ($R^2 = 0.9972$). The slope of the trend line is 195.13 ppm/°C, which is slightly higher than the simulated K_T value of 192.45 ppm/°C. The normalized deviation between the simulated and experimental K_T is 1.39%.

VII. Conclusion

In this paper, a wireless temperature sensor consisting of only microstrip circuit elements and has no other electronic components is demonstrated. A wireless interrogation system that is capable of acquire the sensing signal in the far field of the wireless antenna sensor was developed. Temperature testing up to 280°C was conducted to validate the functionalities of the wireless sensor and its interrogation system. The measured temperature sensitivity of 195.13 ppm/°C matches very well with the theoretical prediction. We selected the patch antenna as the sensing element in this study primarily because of its unique advantages, such as easy of fabrication, multi-sensing modality, etc. However, the presented technique can be applied to any other temperature sensitive microwave resonators as well. In the future, an alternative wireless interrogator will be investigated to reduce the interrogator cost and to increase the interrogation speed. In addition, a commercial PCB substrate was selected in this study for the proof-of-concept purpose. We are currently exploring customized high-temperature PCB material to increase the operation temperature of the wireless antenna sensor.

Disclaimer

This report was prepared as an account of work sponsored by an agency of the United States Government. Neither the United States Government nor any agency thereof, nor any of their employees, makes any warranty, express or implied, or assumes any legal liability or responsibility for the accuracy, completeness, or usefulness of any information, apparatus, product, or process disclosed, or represents that its use would

not infringe privately owned rights. Reference herein to any specific commercial product, process, or service by trade name, trademark, manufacturer, or otherwise does not necessarily constitute or imply its endorsement, recommendation, or favoring by the United States Government or any agency thereof. The views and opinions of authors expressed herein do not necessarily state or reflect those of the United States Government or any agency thereof.

REFERENCES

[1] P. R. N. Childs, J. R. Greenwood, and C. A. Long, "Review of temperature measurement," *Rev. Sci. Instrum.*, vol. 71, no. 8, pp. 2959–2978 2000.

[2] B. Lee, "Review of the present status of optical fiber sensors," *Opt. Fiber Technol.*, vol. 9, no. 2, pp. 57–79, 2003.

[3] Q. Tan *et al.*, "Antenna-resonator integrated wireless passive temperature sensor based on low-temperature co-fired ceramic for harsh environment," *Sens. Actuators A, Phys.*, vol. 236, pp. 299–308, Dec. 2015.

[4] F. Sivrikaya and B. Yener, "Time synchronization in sensor networks: A survey," *IEEE Netw.*, vol. 18, no. 4, pp. 45–50, Jul./Aug. 2004.

[5] I. F. Akyildiz, W. Su, Y. Sankarasubramaniam, and E. Cayirci, "A survey on sensor networks," *IEEE Commun. Mag.*, vol. 40, no. 8, pp. 102–114, Aug. 2002.

[6] J. Yick, B. Mukherjee, and D. Ghosal, "Wireless sensor network survey," *Comput. Netw.*, vol. 52, no. 12, pp. 2292–2330, Aug. 2008.

[7] A. P. Sample, D. J. Yeager, P. S. Powledge, A. V. Mamishev, and J. R. Smith, "Design of an RFID-based battery-free programmable sensing platform," *IEEE Trans. Instrum. Meas.*, vol. 57, no. 11, pp. 2608–2615, Nov. 2008.

[8] F. Kocer and M. P. Flynn, "An RF-powered, wireless CMOS temperature sensor," *IEEE Sensors J.*, vol. 6, no. 3, pp. 557–564, Jun. 2006.

[9] L. M. Reindl and I. M. Shrena, "Wireless measurement of temperature using surface acoustic waves sensors," *IEEE Trans. Ultrason., Ferroelectr., Freq. Control*, vol. 51, no. 11, pp. 1457–1463, Nov. 2004.

[10] D. Girbau, A. Ramos, A. Lazaro, S. Rima, and R. Villarino, "Passive wireless temperature sensor based on time-coded UWB chipless RFID tags," *IEEE Trans. Microw. Theory Techn.*, vol. 60, no. 11, pp. 3623–3632, Nov. 2012.

[11] D. J. Thomson, D. Card, and G. E. Bridges, "RF cavity passive wireless sensors with time-domain gating-based interrogation for SHM of civil structures," *IEEE Sensors J.*, vol. 9, no. 11, pp. 1430–1438, Nov. 2009.

[12] J.-M. Boccard, T. Aftab, J. Hoppe, A. Yousaf, R. Hütter, and L. M. Reindl, "High-resolution, far-field, and passive temperature sensing up to 700 °C using an isolated ZST microwave dielectric resonator," *IEEE Sensors J.*, vol. 16, no. 3, pp. 715–722, Feb. 2016.

[13] H. Cheng, S. Ebadi, and X. Gong, "A low-profile wireless passive temperature sensor using resonator/antenna integration up to 1000 °C," *IEEE Antennas Wireless Propag. Lett.*, vol. 11, pp. 369–372, Apr. 2012.

[14] H. Kairm *et al.*, "Concept and model of a metamaterial-based passive wireless temperature sensor for harsh environment applications," *IEEE Sensors J.*, vol. 15, no. 3, pp. 1445–1452, Mar. 2015.

[15] Q. Tan *et al.*, "Wireless passive temperature sensor realized on multilayer HTCC tapes for harsh environment," *J. Sensors*, vol. 2015, Oct. 2015, Art. no. 124058.

[16] H. Huang, "Flexible wireless antenna sensor: A review," *IEEE Sensors J.*, vol. 13, no. 10, pp. 3865–3872, Oct. 2013.

[17] A. Deivasigamani, A. Daliri, C. H. Wang, and S. John, "A review of passive wireless sensors for structural health monitoring," *Mod. Appl. Sci.*, vol. 7, no. 2, pp. 57–76, 2013.

[18] S. Deshmukh and H. Huang, "Wireless interrogation of passive antenna sensors," *Meas. Sci. Technol.*, vol. 21, no. 3, p. 035201, 2010.

[19] X. Yi, T. Wu, Y. Wang, R. T. Leon, M. M. Tentzeris, and G. Lantz, "Passive wireless smart-skin sensor using RFID-based folded patch antennas," *Int. J. Smart Nano Mater.*, vol. 2, no. 1, pp. 22–38, 2011.

[20] Q. Qiao, L. Zhang, F. Yang, Z. Yue, and A. Z. Elsherbeni, "Reconfigurable sensing antenna with novel HDPE-BST material for temperature monitoring," *IEEE Antennas Wireless Propag. Lett.*, vol. 12, pp. 1420–1423, 2013.

[21] M. Hasani, A. Vena, L. Sydanheimo, L. Ukkonen, and M. M. Tentzeris, "Implementation of a dual-interrogation-mode embroidered RFID-enabled strain sensor," *IEEE Antennas Wireless Propag. Lett.*, vol. 12, pp. 1272–1275, 2013.

[22] J. Yao, S. Tjuatja, and H. Huang, "Real-time vibratory strain sensing using passive wireless antenna sensor," *IEEE Sensors J.*, vol. 15, no. 8, pp. 4338–4345, Aug. 2015.

[23] H. Cheng, S. Ebadi, X. Ren, and X. Gong, "Wireless passive high-temperature sensor based on multifunctional reflective patch antenna up to 1050 degrees centigrade," *Sens. Actuators A, Phys.*, vol. 222, pp. 204–211, Feb. 2015.

[24] A. Daliri, A. Galehdar, W. S. T. Rowe, S. John, C. H. Wang, and K. Ghorbani, "Quality factor effect on the wireless range of microstrip patch antenna strain sensors," *Sensors*, vol. 14, no. 1, pp. 595–605, 2014.

[25] J. W. Sanders, J. Yao, and H. Huang, "Microstrip patch antenna temperature sensor," *IEEE Sensors J.*, vol. 15, no. 9, pp. 5312–5319, Sep. 2015.

[26] H. Mosallaei and K. Sarabandi, "Antenna miniaturization and bandwidth enhancement using a reactive impedance substrate," *IEEE Trans. Antennas Propag.*, vol. 52, no. 9, pp. 2403–2414, Sep. 2004.

[27] L.-W. Li, Y.-N. Li, T. S. Yeo, J. R. Mosig, and O. J. Martin, "A broadband and high-gain metamaterial microstrip antenna," *Appl. Phys. Lett.*, vol. 96, no. 16, p. 164101, 2010.

[28] C. Balanis, *Antenna Theory: Analysis and Design*, 3rd ed. New York, NY, USA: Wiley, 2005.

[29] *RO3000 Series Circuit Materials Datasheet*, Rogers Corp., Rogers, CT, USA, 2011.

[30] H. Huang and T. Bednorz, "Introducing S-parameters for ultrasound-based structural health monitoring," *IEEE Trans. Ultrason., Ferroelectr., Freq. Control*, vol. 61, no. 11, pp. 1856–1863, Nov. 2014.

Jun Yao was born in Jiangsu, China, in 1986. He received the M.S. degree in electrical engineering from the University of Shanghai for Science and Technology, Shanghai, China, in 2012. He is currently pursuing the Ph.D. degree with the Department of Electrical Engineering, University of Texas at Arlington. His research interests include wireless sensor technology for structural health monitoring, IC circuit design for RF energy harvester and antenna interrogation, and digital signal processing.

Franck Mbanya Tchafa received the M.Eng. (Hons.) degree in aerospace engineering from the City University of London, London, U.K., in 2010. He is currently pursuing the Ph.D. degree with the Department of Mechanical and Aerospace Engineering, University of Texas at Arlington. His research interests cover wireless sensor technology and the design and analysis of distributed antenna sensors for structural health monitoring.

Ankur Jain received the B.Tech. degree from the Indian Institute of Technology, Delhi, in 2001, and the M.S. and Ph.D. degrees from Stanford University, in 2003 and 2007, respectively, all in mechanical engineering. He is currently an Assistant Professor of Mechanical and Aerospace Engineering with the Microscale Thermophysics Laboratory, University of Texas at Arlington, where he is the Director of Mechanical and Aerospace Engineering. His research interests include thermal measurements, energy conversion and sustainability, heat transfer, and electrochemistry. He is a recipient of the NSF CAREER Award (2016) and the ASME Electronics and Photonics Packaging Division Young Engineer of the Year Award (2013).

Saibun Tjuatja (SM'03) received the B.S.E.E. degree from the University of Texas at Arlington (UTA), the M.S.E.E. degree from Purdue University, and the Ph.D. degree in electrical engineering from UTA. He is currently an Associate Professor and Director of the Wave Scattering Research Center, Department of Electrical Engineering, UTA, where he has been a Faculty Member since 1993. His current research interests include wave propagation and scattering in random media, remote sensing and radar imaging, subsurface sensing, and wireless structural health monitoring. He is a member of Tau Beta Pi and Sigma Chi, and a Fellow of the Electromagnetic Academy.

Haiying Huang (M'98) received the B.Eng. degree in aircraft propulsion from the Beijing University of Aeronautics and Astronautics in 1987, the M.S. degree in electrical engineering and the Ph.D. degree in aerospace engineering from the Georgia Institute of Technology, in 1997 and 1998, respectively. She is a Professor of Mechanical and Aerospace Engineering with the University of Texas at Arlington. Her current research interests are focused on developing wireless, microwave, ultrasonic, and optical fiber sensors for structural health monitoring. She is a recipient of the NSF CAREER Award (2009).